ISBN: 978-3-95450-233-2 ISSN: 2673-5504 doi:10.18429/JACoW-SRF2021-WEPFDV004

A NEW MODEL FOR Q-SLOPE IN SRF CAVITIES: RF HEATING AT MULTIPLE JOSEPHSON JUNCTIONS DUE TO WEAKLY-LINKED GRAIN BOUNDARIES OR DISLOCATIONS*

K. Saito†, Facility for Rare Isotope Beams, Michigan State University, East Lansing, MI, USA

Abstract

Several models have already been proposed for the medium field *Q*-slope (MFQS) and high field *Q*-slope (HFQS) in SRF cavities. However, the existing models do not explain both MFQS and HFQS in a unified way. A new model with multiple Josephson junctions at weakly-linked grain boundaries or dislocations is proposed for a unified explanation of both effects. The new model incorporates two kinds of junction: ceramic-like junctions for MFQS, and weak superconductor junctions for HFQS. In measurements of RF power dissipation (P_{loss}) versus RF field, an increase in P_{loss} proportional to the cube of the field is observed for MFQS. This is seen for cavities prepared with both buffered chemical polishing (BCP) and electropolishing (EP). An exponential increase in P_{loss} with field is often observed at high field for BCP'ed cavities (HFQS). If the number of Josephson junctions increases linearly with the RF field, as expected due to flux quantum penetration, these behaviors are easily explained. In addition, the new model can potentially explain the anti-*Q* slope behavior observed in nitrogen-doped or mid-temperature-baked cavities. In this paper, the new model will be described and compared with measurements.

MOTIVATION

The Facility for Rare Isotope Beams (FRIB) at Michigan State University (MSU) is a collaborative project with the US Department of Energy for research at the frontiers of nuclear science. A total of 324 superconducting resonators were fabricated, tested, and installed into the FRIB driver linac: 2 types of quarter-wave resonators (QWRs) at 80.5 MHz and 2 types of half-wave resonators (HWRs) at 322 MHz. First acceleration of ion beams through the full linac was achieved in May 2021 [1].

Analyses of Dewar certification testing results for FRIB cavities has been undertaken [2]. The cavities were prepared with buffered chemical polishing (BCP) but no low temperature bake (LTB).

Many of the FRIB cavities showed high field *Q*-slope (HFQS). An example is shown in Fig. 1: pure HFQS is seen with no field emission (FE) X-rays up to the maximum field. In the data analysis, a Fowler-Nordheim (FN) analysis was applied to the HFQS. FN analysis is usually applied to FE analysis [3], rather than HFQS. The FN model describes FE as an electron tunneling effect. The good FN fitting results for pure HFQS (Fig. 2) suggests that a quasi-electron tunneling mechanism can explain HFQS, which led us to consider the Josephson Effect [4].

Measurements of the accelerating gradient (E_{acc}) as a function of Q_0 (intrinsic quality factor) are often analyzed in terms of the RF surface resistance. For the FRIB cavities' MFQS, we took a different approach: we considered P_{loss} as the sum of contributions from various mechanisms. We observed an increase in RF power dissipation (P_{loss}) as the cube of the RF field for the FRIB cavities. An example is shown in Fig. 3: below the HFQS threshold, P_{loss} closely follows a cubic dependence on the peak surface electric field (E_p), as indicated by the black line.

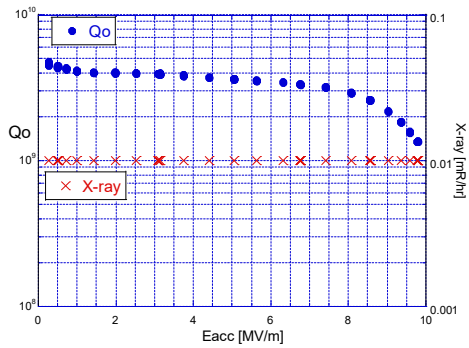

Figure 1: Quality factor as a function of accelerating gradient for a FRIB β = 0.29 HWR at 2 K.

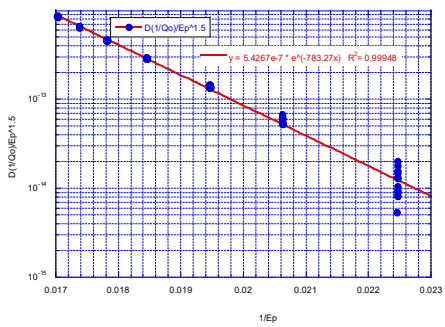

Figure 2: FN plot for the HFQS of Fig.1.

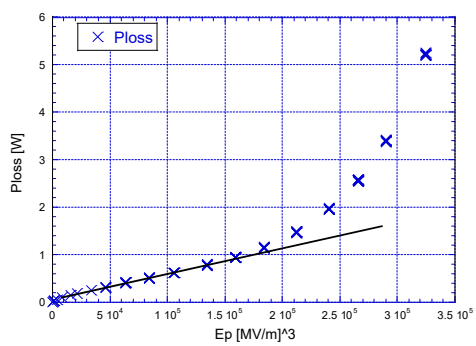

Figure 3: Power dissipation as a function of the cube of the peak surface electric field.

* Work supported by the U.S. Department of Energy Office of Science DE-S0000661 and the National Science Foundation under Cooperative Agreement PHY-1102511
† saito@frib.msu.edu

ISBN: 978-3-95450-233-2 ISSN: 2673-5504 doi:10.18429/JACoW-SRF2021-WEPFDV004

JOSEPHSON EFFECT

The Josephson Effect refers to Cooper pair current (supercurrent) or quasi-electron current (normal current) tunnelling through a barrier, known as a Josephson junction (JJ). Figure 4 (left) shows an example in which two superconductors are separated by a thin insulating layer. The junction can consist of a thin insulator, a short section of normal-conducting metal, or a physical constriction that weakens the superconductivity at the point of contact. For a microwave current $J_{RF} < I_c$ (critical current), the Cooper pair current flows without any voltage (in this case RF emission happens); for $J_{RF} > I_c$, quasi-electrons flow with a voltage, which produces resistive losses (Fig. 4, right). More information about the Josephson Effect can be found in Ref. [4].

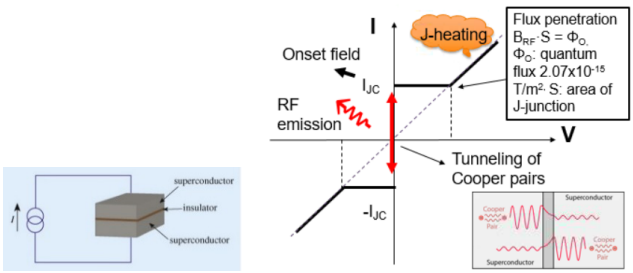

Figure 4: Left: Josephson junction example. Right: JJ current as a function of voltage.

RF DISSIPATION AT WEAKLY-LINKED GRAIN BOUNDARIES

A weakly-linked grain boundary, illustrated in Fig. 5, can be modelled as a JJ. With an RF current $J_{RF} > I_c$, the current flows across the junction. The flux produced by J_{RF} satisfies the flux penetration condition:

$$B_{RF} \cdot S = n \cdot \Phi_0 \quad , \tag{1}$$

where S is the area of the JJ, Φ_0 is the quantum fluxiod = 2.07×10^{-15} T·m^2, and n is an integer. When J_{RF} flows across a JJ within the penetration depth (λ) on the top SRF surface, as illustrated in Fig. 6, a voltage V_J is required. As a result, RF heating (p_J) at the JJ ("J-heating") is produced:

$$p_J = V_J \cdot J_{RF} \propto E_p^2 \quad , \tag{2}$$

where E_p is the surface electric field. We assume multiple JJs on the SRF surface. If the total number of JJs is N, then the total J-heating power (P_J) is

$$P_J = N \cdot p_J \quad . \tag{3}$$

This J-heating will contribute to the Q-slope.

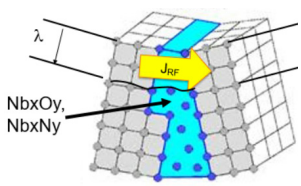

Figure 5: RF current flow at a weakly-linked grain boundary.

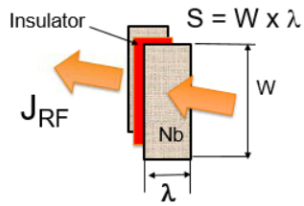

Figure 6: Insulating JJ with size $S = W \cdot \lambda$, where λ is the field penetration depth.

B. Bonin and H. Safa at Saclay proposed a Josephson array model for RF dissipation on polycrystalline cavities in 1991 [5]; however they did not do a detailed analysis for Nb SRF cavities. The model proposed here is intended for a quantitative data analysis, done by assuming the number of JJs (N) is proportional to the RF field. The flux penetration condition, Eq. (1), means that a higher field produces a smaller JJ. Thus, it is reasonable to assume that N increases linearly with the field, which leads to the E_p^3 dependence in the RF dissipation described above.

We have asserted that the weak links responsible for MFQS are insulating JJs, and HFQS is due to weak superconductor JJs. Both Q-slopes have their own onset field (E_M or E_H).

For the J-heating responsible for MFQS, we can write

$$P_J \propto (E_p - E_M)^2 \cdot E_p \quad . \tag{4}$$

The number of JJs contributing to HFQS increases exponentially with field because of the superconducting break at the RF magnetic field above the onset field. For HFQS, we can write

$$P_J \propto (E_p - E_H)^2 \cdot E_p \exp[C \cdot (E_p - E_H)] \quad , \tag{5}$$

where C is a constant.

We provide several equations below derived from basic physical parameters:

$$B\ (\text{onset}) = \frac{\phi_0}{S} = (B_p/E_p) \cdot C_2 \tag{6}$$

$$W = \frac{S}{\lambda} = \frac{\phi_0}{\lambda \times B(onset)} \quad , \tag{7}$$

where W is the size of the insulator, per Fig. 6.

$$J_{JC} = J_{RF}\ (\text{onset}) = \frac{W \times B_p(onset)}{\mu_0} = \frac{\phi_0}{\lambda \mu_0} \tag{8}$$

$$J_{RF} = \frac{W \times B_p}{\mu_0} = \frac{W}{\mu_0} \cdot (B_p/E_p) \cdot E_p, \ \mu_0 = 1.26 \times 10^{-6} \tag{9}$$

$$p_J = \frac{f \phi_0}{2 J_{JC}} \times (J_{RF} - J_C)^2 \quad . \tag{10}$$

BIG PICTURE OF THE MODEL

The new model has the potential to describe various Q-slope behaviours. By a simple calculation, the E_p^3 dependence of the RF dissipation for the MFQS give a quality factor Q_0* of

$$Q_0^* = \frac{Q_0}{(1 + a \cdot E_{acc})} \quad . \tag{11}$$

ISBN: 978-3-95450-233-2 ISSN: 2673-5504 doi:10.18429/JACoW-SRF2021-WEPFDV004

where a is a constant and Q_0 is the field-independent quality factor from the BCS and residual contributions to the RF surface resistance.

The model includes RF emission for $J_{RF} < I_c$. In this case, the emitted energy (ΔU) adds to the stored energy (U). The emission energy (u) at one JJ is proportional to the field: $u \propto E_p^2$. The total emission energy from multiple JJ is then

$$\leftrightarrows U = N \times u \propto E_p^3 \quad . \tag{12}$$

By a simple calculation, the quality factor with RF emission is

$$Q_0{}^* = Q_0 \times (1 + \Rightarrow \cdot \mathrm{Eacc}) \quad . \tag{13}$$

Equation (15) describes an anti-Q-slope.

Thus, the new model can explain multiple Q-slope behaviours: MFQS, HFQS, anti-Q-slope, hydrogen disease, etc. Figure 7 provides some examples based on the equations shown above.

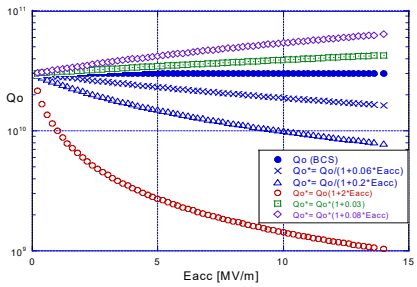

Figure 7: Some Q-slope behaviours described by the model.

EXAMPLE OF DATA ANALYSIS

As an example, we consider measurements on a FRIB HWR (β = 0.29, S29-009). The RF parameters of this cavity are listed in Table 1. FRIB cavities are BCP'ed to remove about 120 µm, hydrogen degassed at 600 °C for 10 hrs, and light etched without low temperature baking.

2 K Data Analysis

The cavity performance at 2 K is shown in Fig. 8 (left). This cavity had no X-rays up to the maximum field. No thermal feedback mechanism is included in the analysis, because liquid helium has no boiling below the Lambda point (2.17 K). The HFQS onset field (E_H) was first estimated from P_{loss} vs E_p, as shown in Fig. 8 (right). The BCS contribution was then estimated by fitting the lowest-field measurements to an E_p^2 dependence (requiring $P_{loss} = 0$ at $E_p = 0$), as seen in Fig. 9 (left). The third step was to fit the MFQS, as shown in Fig. 9 (right). Finally the HFQS fitting was done as shown in Fig. 10 (left). All of the heating contributions are shown in Fig. 10 (right), along with their sum:

$$P_{loss} = \text{BCS-heating} + \text{J-heating} + \text{HFQS-heating}$$
$$= 9.6817\text{E-}4 \cdot E_p^2 + 6.8864\text{E-}6 \cdot (E_p - E_M)^2 \cdot E_p +$$
$$4.589\text{E-}7 \cdot (E_p - E_H)^2 \cdot E_p \cdot \exp[79.997 \cdot (E_p - E_H) \cdot 1.7907\text{E-}3] \,,$$

with $E_M = 2.0672$ MV/m and $E_H = 27.83$ MV/m.

Table 1: RF Parameters for FRIB β = 0.29 HWRs

β	0.29
Frequency	322 MHz
V_{acc}	2.09 MV
U/E_p^2	8.657 mJ/(MV/m)^2
E_p/E_{acc}	4.3
B_p/E_{acc}	7.7 mT/(MV/m)
R_{acc}/Q_0	224.4 ⌄
Geometry factor ↓↑	77.9 ⌄

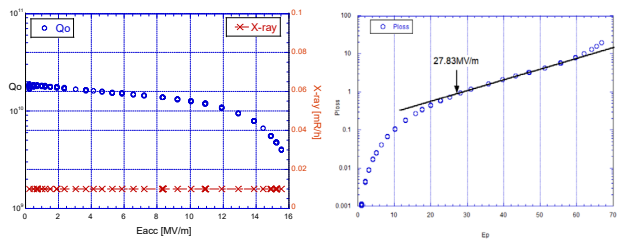

Figure 8: Left: cavity performance at 2 K. Right: onset field for HFQS.

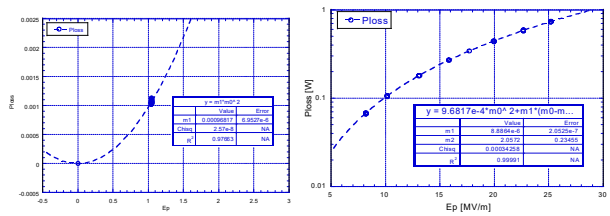

Figure 9: Fit for BCS losses (left) and MFQS (right).

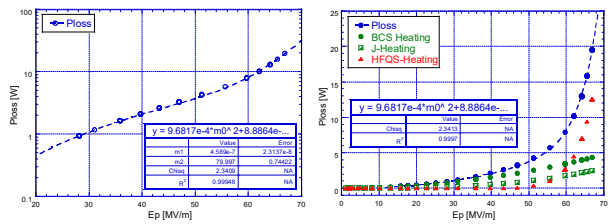

Figure10: HFQS fitting (left); fitted contributions and sum (right).

4.3 K Data Analysis

At 4.3 K, the thermal feedback mechanism must be considered. This contribution is approximated by multiplying E_p^2 to P_{loss}. HFQS is not seen in the 4.3K measurements, which were limited by available RF power. Contributions to P_{loss} are BCS-heating, MFQS, and thermal feedback, as shown in Fig.11 (left). The cavity had no field emission X-rays at 4.3 K. Fig 11 (right) compares the measured data and fitted curve for Q_0 as a function of field. The fitting result is

$$P_{loss} = (1 + 1.2176\text{E-}3 \cdot E_p^2) \cdot [1.1538\text{E-}2 \cdot E_p^2$$
$$+ 3.2124\text{E-}6 \cdot (E_p - 1.250)^2 \cdot E_p] .$$

ISBN: 978-3-95450-233-2 ISSN: 2673-5504 doi:10.18429/JACoW-SRF2021-WEPFDV004

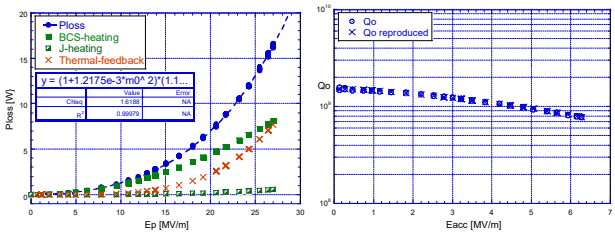

Figure 11: Left: 4.3 K fitted contributions and sum. Right: measured and fitted quality factor at 4.3 K.

ANALYSIS OF BCP'ED AND BAKED CAVITY

The effect of low-temperature baking (LTB) was investigated for FRIB cavities. We found that, at 4.3 K, the LTB improves Q_0 and allows for slightly larger field (Fig. 12, left), but has almost no impact on the performance at 2 K (Fig. 12, right). LTB wasn't done for FRIB production cavities because it was planned to operate them at 2 K, and the benefit was not sufficient to offset the additional time and labour.

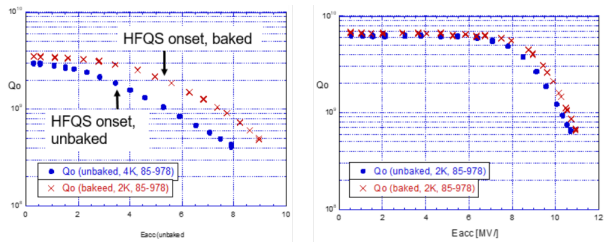

Figure 12: Performance of a FRIB β = 0.085 QWR (S85-978) before and after LTB.

We applied the new model to try to understand the impact of LTB. The analysis results are summarized in Table 2

Table 2: Comparison of Model Parameters before and after Low-Temperature Baking

Parameter	T	Unbaked	Baked
E_M = onset field (E_p) for MFQS (MV/m)	4.3 K	2.13	10.0
	2 K	2.51	7.98
Width of MFQS-JJ (↘m)	4.3 K	7.6	1.6
	2 K	6.6	2.1
J-heating strength (W)	4.3 K	2.75E-5	7.65E-7
	2 K	3.01E-6	302E-6
E_H = onset field (E_p) for HFQS (MV/m)	4.3 K	15.5	19.2
	2 K	35.4	45.4
Width of HFQS-JJ (↘m)	4.3 K	1.05	0.85
	2 K	0.47	0.37
HFQS-heating strength (W)	4.3 K	9.60E-5	3.85E-5
	2 K	1.40E-5	2.51E-5

The conclusions are:

1. The size of MFQS JJs becomes very small after LTB, and the MFQS heating decreases significantly, which is especially noticeable at 4.3 K. At 2 K, the MFQS contribution is small, which results in little difference between unbaked and baked cavities.
2. The size of HFQS JJs follows a trend similar to MFQS, but difference is smaller than for J-heating.
3. At 4.3 K, the HFQS contribution decreases a bit due to the higher onset field.
4. At 2 K, the HFQS contribution is similar between the baked and unbaked cases due to the small difference in the onset.

The decrease in JJ size after LTB is consistent with the oxygen diffusion model. Our model provides an intuitive understanding.

ANALYSIS OF AIR-EXPOSED CAVITY

In past studies at KEK, a β = 0.45, single-cell cavity (1.3 GHz, K-25) was exposed to air for 10 days [6]. After bulk electropolishing (120 μm) and hydrogen degassing (750°C, 3 hrs), the cavity was treated by light EP, high pressure water rinsing (HPR), and LTB (120 °C, 48 hrs) as the baseline. The baseline performance at 1.5 K reached E_p = 66.8 MV/m without X-rays, as shown in Fig. 12 (left, blue circles). For this case, B_p/E_p = 2.57 [7], so B_p reached 174 mT, which is very close to the fundamental limit.

After the baseline test, air was injected into the cavity through a 0.2 μm mesh filter to bring the pressure to 1 atm. After the cavity was left closed for 10 days, HPR was done without LTB, and the 1.5 K test was repeated, as shown in Fig. 13 (left, green circles). A maximum E_p of 55 MV/m was reached without X-rays but significant MFQS was seen. After this test, this cavity underwent a LTB (120°C, 48 hrs) without venting, and a third 1.5 K test was done, as shown in Fig 13 (left, red diamonds). A maximum E_p of 50 MV/m was reached without X-rays. The LTB provided some lessening of the MFQS.

Figure 13 (right) shows P_{loss} as a function of E_p^3 for these three tests. Table 3 summarize the analysis results from the J-heating model.

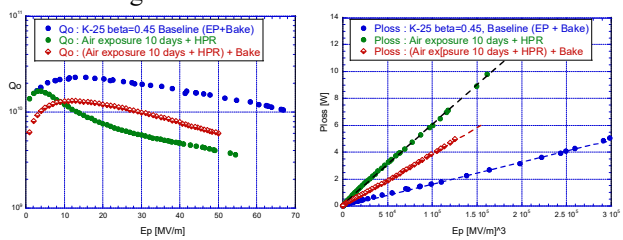

Figure: 13: Impact of air exposure on the performance of a β = 0.45 single cell cavity at 1.5 K.

Table 3: J-Heating Model Analysis of Air Exposure

Parameter	Baseline	Air exposed	After baking
Max E_p (MV/m)	66.8	55.4	50.1
Max B_p (mT)	174.2	142.0	130.5
BCS-heating strength [W/(MV/m)^2]	5.09e-4	8.17e-4	8.57e-4
E_M = J-heating onset E_p (MV/m)	15.3	2.08	12.2
J-heating strength [W/(MV/m)^3]	1.94e-5	4.94e-5	5.08e-5

ISBN: 978-3-95450-233-2 ISSN: 2673-5504 doi:10.18429/JACoW-SRF2021-WEPFDV004

The new model tells us that the air exposure decreases the onset of J-heating significantly, resulting in a significantly larger MFQS (J-heating) contribution. Baking mitigates this impact by pushing the J-heating onset back up.

ANTI-Q-SLOPE BEHAVIOUR

The previous three analyses were for RF dissipation for the case of $J_{RF} > I_C$, however, the model predicts an anti-Q-slope behaviour due to RF emission when $J_{RF} < I_C$. Usually I_C is very small and the anti-Q-slope behaviour is difficult to observe in a wide range. However, if the insulating layer becomes very thin, I_C can become large, producing a clear anti-Q-slope. A model calculation gives [8]

$$I_C = (q_s\hbar\sqrt{n_{s1}n_{s2}})/[m_s \cdot \sinh(2d/\gamma)] \quad , \qquad (14)$$

where q_s is Cooper pair charge; n_{s1} and n_{s2} are the densities of Cooper pairs in superconductor 1 and 2, respectively; m_s is the mass of the Cooper pair; γ is a damping constant of the wave function in the insulator (several nm, according to measurements), and $2d$ is the thickness of the JJ insulating layer. In general, for small x,

$$\sinh(x) \approx \frac{2x}{1-x^2} \sim 2x \quad . \qquad (15)$$

hence, for $2d << \gamma$, I_C will increase inversely with the insulator thickness. The thickness of the weakly-linked grain boundaries at the cavity surface could be reduced by treatments such as titanium or nitrogen doping or by mid-temperature baking (MTB).

As explained above, the quality factor in the anti-Q-slope case may be described by Equation (13): the model predicts that the quality factor will increase linearly with the RF field. Figure 14 shows Ti-doping results for a large-grain Nb cavity studied by P. Dhakal *et al*. at Jlab [9]. The measured quality factor is plotted on a linear scale. The linear field dependence is observed up to B_p= 40 mT. Above 40 mT, Q_0 begins to decrease exponentially, possibly due to HFQS.

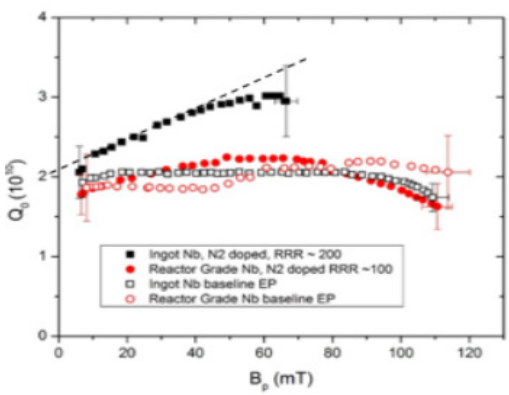

Figure 14: Solid black squares: performance of a Ti-doped cavity [9]. Dashed line: linear fit using our model.

Figure 15 shows result of MTB by S. Posen et al at FNAL [10], again, with a linear scale for the quality factor. Though there is some variation from the predicted dependence, the overall anti-Q-slope is a good fit to the expected linear field dependence of Q_0 on field.

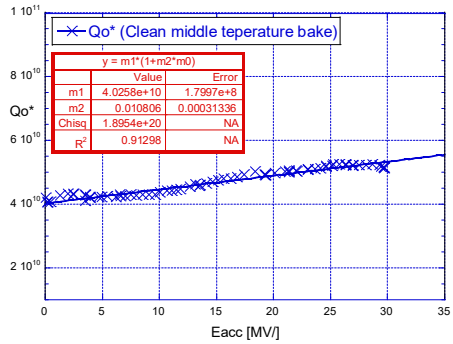

Figure 15: Blue crosses: performance of an Nb cavity after mid-temperature baking [10]. Solid line: linear fit using our model.

CONCLUSION

A model has been developed which can explain various SRF cavity behaviours: medium-field Q-slope, high-field Q-slope, anti-Q-slope, effects from baking, air exposure, etc. The model is simple and intuitive.

ACKNOWLEDGEMENTS

Certification cold-tests for the FRIB production resonators were done by W. Hartung, J. Popielarski, Sang-hoon Kim, Wei Chang, and C. Zhang. W. Hartung established the data base of test results which was used for the cavity data analysis. The author appreciates their efforts very much.

REFERENCES

[1] T. Xu *et al.*, "Completion of FRIB Superconducting Linac and Phased Beam Commissioning," presented at SRF2021, Virtual, June 2021, paper MOOFAV10, this conference.

[2] C. Zhang *et al.*, "Certification Testing of Production Superconducting Quarter-Wave and Half-Wave Resonators for FRIB," *Nucl. Instrum. Methods*. vol. 1014, p.165675, Oct. 2021. doi:10.1016/j.nima.2021.165675

[3] S. Noguchi *et al.*, "Measurement of a superconducting 500 MHz Nb cavity in the TM010-Mode," *Nucl. Instrum. Methods*, vol 179, p. 205-215, 1981. doi:10.1016/0029-554X(81)90041-0

[4] B. D. Josephson, "Possible new effects in superconductive tunnelling," *Phys. Lett.*, vol. 1, p. 251–253, Jul. 1962. doi:10.1016/0031-9163(62)91369-0

[5] B. Bonin and H. Safa, "Power dissipation and Technology for high field in granular RF Superconductivity," *Supercond. Sci. Technol.*, vol. 4, No. 6, pp.257-261, Feb. 1991. doi:10.1088/0953-2048/4/6/008

[6] K. Saito, "Behaviour of Air Exposure of Medium β (=0.45) Niobium SC Cavity," in *Proc. 10th Workshop RF Superconductivity (SRF'01)*, Tsukuba, Japan, Sep. 2001, paper PH004, pp. 588-590. https://jacow.org/srf01/papers/ph004.pdf

[7] K. Saito *et al.*, "Development of 1.3 GHz Medium-β Structure with High Gradient", in *Proc. 8th Int. Conf. RF Superconductivity (SRF'97)*, Abano Terme (Padova), Italy, Oct. 1997, paper SRF97C15, pp. 534-539. https://jacow.org/SRF97/papers/srf97c15.pdf

[8] MIT, 6.763 2003 Lecture 11 https://web.mit.edu/6.763/www/FT03/Lectures/Lecture11.pdf

ISBN: 978-3-95450-233-2 ISSN: 2673-5504 doi:10.18429/JACoW-SRF2021-WEPFDV004

[9] P. Dhakal, G. Ciovati, P. Kneisel, and G. R. Myneni, "Enhancement in Quality Factor of SRF Niobium Cavities by Material Diffusion," *IEEE Trans. Appl. Supercond.*, vol. 25, no.3, p. 3500104, June 2015. doi:10.1109/TASC.2014.2359640

[10] S. Posen, A. Romanenko, A. Grassellino, and D.A Sergatskov, "Ultralow Surface Resistance via Vacuum Heat Treatment of Superconducting Radio-Frequency Cavities," *Phys. Rev. Appl.,* vol. 13, p. 014024, Jun. 2019. doi:10.1103/PhysRevApplied.13.014024

.